31 March 1995

ELSEVIER

Chemical Physics Letters 235 (1995) 484–489

CHEMICAL PHYSICS LETTERS

Study of the predissociation of CH_3O $\tilde{A}(^2A_1)$ by fast beam photofragment translational spectroscopy

David L. Osborn [a,b,1], David J. Leahy [a,b], Eric M. Ross [a,b], Daniel M. Neumark [a,b,2]

[a] *Department of Chemistry, University of California, Berkeley, CA 94720, USA*
[b] *Chemical Sciences Division, Lawrence Berkeley Laboratory, Berkeley, CA 94720, USA*

Received 30 November 1994; in final form 24 January 1995

Abstract

The dissociation dynamics of the methoxy radical (CH_3O) following excitation of the $\tilde{A}(^2A_1) \leftarrow \tilde{X}(^2E)$ transition are examined using photofragment translational spectroscopy. The radicals are produced from photodetachment of a fast, cold negative ion beam. We find that levels of the $\tilde{A}$ state are strongly predissociated starting with $\nu_3 = 6$ at 35419 cm^{-1} excitation energy. Three product channels are identified: (1) $CH_3 + O$, (2) $CH_2 + OH$, and (3) $CH_2O + H$, with channel (1) by far the dominant channel. In channel (1), resolved vibrational structure of the methyl fragment is seen in the translational energy distribution, providing insight into the dissociation dynamics of CH_3O. Several thermodynamics quantities are also obtained: $D_0(CH_3\text{–}O) = 87.8 \pm 0.3$ kcal/mol, $\Delta H^0_{f,0}(CH_3O) = 6.8 \pm 0.4$, $D_0(CH_3O\text{–}H) = 104.0 \pm 0.5$, $\Delta H_{acid,0}(CH_3O\text{–}H) = 381.4 \pm 0.7$, and $D_0(H\text{–}CH_2O) = 19.8 \pm 0.4$.

Photodissociation experiments are a powerful means of investigating the dissociation dynamics and potential energy surfaces of small molecules. While the majority of chemical systems so studied have been closed-shell molecules, these experiments offer considerable promise in unraveling the complicated electronic and nuclear dynamics of free radicals. By production of well-characterized radicals through photodetachment of a fast beam of negative ion precursors, we have extended photodissociation in a general way to the study of these important chemical species. Results are presented here for the methoxy radical, CH_3O.

As a prototypical small free radical, CH_3O has been the subject of numerous investigations since its first observation in 1953 [1]. It is the smallest of the alkoxy radicals, an important family of combustion intermediates, and is of considerable spectroscopic interest because of its Jahn–Teller active ^2E ground state and low-lying $\tilde{A}(^2A_1)$ excited state. The spectroscopy [2–13] and reactivity [14,15] of CH_3O has been extensively discussed by many authors. The low-lying dissociative surfaces of CH_3O and their influence on dynamics of the $\tilde{A}$ state have received less attention. Jackels [16] has investigated this issue with ab initio calculations, while Inoue et al. [6], Fuke et al. [7], and Lin and Lee [13] have obtained indirect experimental evidence for predissociation of the $\tilde{A}$ state. In this Letter, we present the first observation of photofragments from predissociation

[1] NDSEG Predoctoral Fellow.
[2] Camille and Henry Dreyfus Teacher–Scholar.

SSDI 0009-2614(95)00151-4

of the methoxy radical following excitation of the $\tilde{A}(^2A_1) \leftarrow \tilde{X}(^2E)$ transition. Our results offer new information about the excited state potential energy surfaces, dissociation dynamics, spectroscopy, and thermodynamics of CH_3O.

The electronically similar OH radical predissociates above $v' = 2$ in its excited $A(^2\Sigma^+)$ state [17]. One might expect to see the analogous channel in CH_3O,

$$CH_3O\ \tilde{X}(^2E) + h\nu \rightarrow CH_3O\ \tilde{A}(^2A_1) \rightarrow CH_3\ \tilde{X}(^2A''_2) + O(^3P), \quad (1)$$

but the methoxy radical has several other thermodynamically feasible dissociation pathways, the most prominent of which are

$$CH_3O\ \tilde{X}(^2E) + h\nu \rightarrow CH_2\{\tilde{X}(^3B_1) \text{ or } \tilde{a}(^1A_1)\} + OHX(^2\Pi), \quad (2)$$

$$CH_3O\ \tilde{X}(^2E) + h\nu \rightarrow CH_2O\ \tilde{X}(^1A_1) + H(^2S). \quad (3)$$

Our results confirm the presence of channel (1) as the major product channel at all energies studied. Channel (2) is also observed at high excitation energy, while channel (3) is detected at high energy in CD_3O.

The fast radical beam translational spectrometer has been described in detail elsewhere [18–20], but a brief description will be given here. We prepare a well-characterized beam of CH_3O radicals by photodetachment of the corresponding negative ion. CH_3O^- is formed during an electric discharge in a pulsed supersonic expansion of 5 atm neon bubbled through CH_3OH. The ions are accelerated to high laboratory energies, mass selected, and photodetached with a pulsed dye laser at 724 nm, just above the detachment threshold [21]. All remaining ions are deflected out of the beam, leaving an internally cold, high velocity packet of neutral CH_3O. These radicals are intersected by the frequency-doubled output of a second dye laser which is tuned from 250–285 nm, covering the $\nu_3 = 6$–13 range of the $\tilde{A}(^2A_1) \leftarrow \tilde{X}(^2E)$ band.

Photofragments recoil out of the beam and are detected without an ionization step by a 46 mm diameter microchannel plate detector 2 m downstream from the photodissociation region. Undissociated radicals are blocked by an 8 mm wide beam

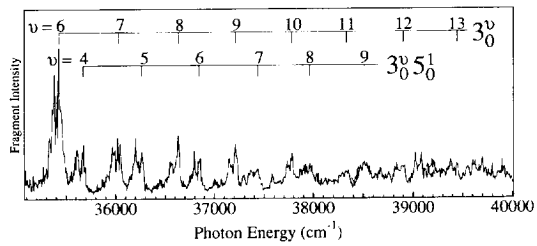

Fig. 1. Total photodissociation cross section of the CH_3O $\tilde{A}(^2A_1) \leftarrow \tilde{X}(^2E)$ transition. Each progression is split by the 60 cm^{-1} spin–orbit splitting of the $\tilde{X}(^2E)$ state.

block across the center of the detector face. Two types of experiments are performed to characterize a photodissociation process. First, the total flux of photofragments is collected as a function of dissociation laser wavelength. Next, we excite a particular transition, measuring the position of the two fragments on the detector face and the time difference between their arrival using a coincidence wedge- and strip-anode detector [20,22]. These quantities yield the magnitude and direction of the center-of-mass relative recoil velocity vector. After correcting for the geometric acceptance of the detector [20], we obtain, for each product channel, the fragment masses, branching ratios, and the center of mass coupled translational energy and angle distribution, $P(E_T, \theta)$. The energy resolution is 25 meV fwhm for 1 eV recoil of $CH_3 + O$.

The results of our total photodissociation cross section measurements are shown in Fig. 1. No predissociation was observed at lower frequencies than those shown in the figure. The spectrum consists of two prominent vibrational progressions superimposed on a weak continuum of fragment signal which slowly rises with increasing excitation energy. The assignment of both progressions is quite straightforward, based on previous absorption [5] and fluorescence [9] studies of CH_3O. Both involve the ν_3 mode of CH_3O, which has a frequency of 660 cm^{-1} in the $\tilde{A}$ state. This mode is primarily a C–O stretch which is active due to the large increase in bond length in the $\tilde{A}(r_{CO} = 1.58\ \text{Å}) \leftarrow \tilde{X}(r_{CO} = 1.37\ \text{Å})$ transition [4]. The main progression is assigned as 3_0^n, whose first member is 3_0^6, at 35419 cm^{-1}. In addition to the pure 3_0^n progression, we observe a strong combination band $3_0^n 5_0^1$ involving excitation of the degenerate ν_5 scissors mode (1407 cm^{-1}).

Because the ν_5 mode has e symmetry, this combination band is nominally forbidden in C_3, symmetry, but is active due to the Jahn–Teller effect in the $\tilde{X}$ state of CH_3O. In addition, each peak shows a splitting on the order of 60 cm^{-1}, the spin–orbit splitting of the $\tilde{X}$ state. The two components have similar intensities because the $^2E_{3/2}$ and the $^2E_{1/2}$ levels are prepared in nearly equal populations by detachment from the negative ion. We note that there are small differences (10–50 cm^{-1}) in the transition frequencies with respect to those in Ref. [9]; these discrepancies will be addressed in a future paper.

Once the wavelength dependence of the total cross section is known, individual vibrational bands are excited at the energies labeled in Fig. 1. From conservation of momentum, the masses of fragments a and b are given by

$$m_{a,b} = M\left[d_{b,a}/(d_b + d_a)\right], \quad (4)$$

where M is the mass of the parent radical and $d_{a,b}$ are the fragment displacements from their center of mass at the detector. Together with position and time information for each event, the data are directly inverted [20,22] to give the translational energy E_T and recoil angle θ relative to the laser polarization. Finally, the doubly differential cross section, $P(E_T, \theta)$, is obtained and separated into energy and angle distributions according to [20,23,24]

$$P(E_T, \theta) = P(E_T)\left[1 + \beta(E_T)P_2(\cos\theta)\right]. \quad (5)$$

Here, $P(E_T)$ is the angle-integrated translational energy distribution, and $\beta(E_T)$ is the anisotropy parameter. These two distributions are easily found from a least-squares fit to $P(E_T, \theta)$.

Fig. 2 shows the photofragment translational energy distributions at several excitation energies. With the exception of the two highest energy transitions, all signal comes from the $CH_3 + O$ channel. In addition, the major feature in every $P(E_T)$ is near the maximum possible energy release. Most of the transitions give rise to well-resolved vibrational structure which can be assigned to the ν_2 umbrella mode (≈ 600 cm^{-1}) of the CH_3 radical. Detailed internal energy distributions are obtained by fitting the data in Fig. 2 to a set of rotational distribution functions spaced by the anharmonic frequencies of the ν_2 mode [25]. The functions we have chosen are nearly Gaussian in shape, with an asymmetric tail

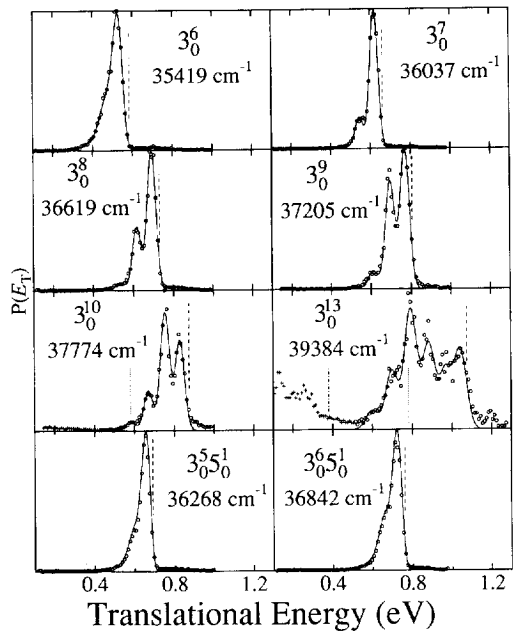

Fig. 2. Center-of-mass translational energy distributions $P(E_T)$ for selected transitions from Fig. 1. Circles show $CH_3 + O$ data, crosses show $CH_2 + OH$ data, while the line represents the model for $CH_3 + O$ (see text). The vertical dashed lines show the maximum possible energy release for $CH_2 + OH$. For 3_0^{10} and 3_0^{13}, the onset of channel (2) is indicated by the dotted line for the CH_2 $\tilde{X}(^3B_1)$ limit and by the dot-dashed line for the $\tilde{a}(^1A_1)$ limit.

extending to higher rotational energy. The partitioning of available energy among fragment translational and internal states is summarized in Table 1. If it is assumed that at least some $v = 0$, $J = 0$ methyl radicals are produced, a single value for D_0, consistent for all data sets, can be found simply by conservation of energy, $D_0 = h\nu - (E_T)_{max} = 87.8 \pm 0.3$ kcal/mol.

In the two $P(E_T)$ distributions at the highest excitation energies (very weakly for the 3_0^{10} band), a second feature is seen at low translational energy, with maximum intensity near zero energy. Using Eq. (4), the data from 0–0.5 eV is found to correspond to masses 14 and 17, i.e. $CH_2 + OH$. Because the fragments from both channels (1) and (2) have nearly the same masses and laboratory energies (≈ 4 keV), their detection efficiency at the microchannel plates are essentially identical. We find the branching ratio of channel (1) to channel (2) is 3 : 1 for the 3_0^{13} band.

Table 1
Excitation energy; partitioning of available energy between translation, vibration, and other internal energy (rotation and spin–orbit); and vibrational branching ratios for each transition shown in Fig. 2

Transition	Energy (cm^{-1})	T (%)	V (%)	Int (%)	$v=0$ (%)	$v=1$ (%)	$v=2$ (%)	$v=3$ (%)	$v=4$ (%)	$v=5$ (%)
3_0^6	35419	81	3	16	84	14	1	0	0	0
3_0^7	36037	88	2	10	82	16	1	0	0	0
3_0^8	36619	86	4	10	67	28	3	1	0	0
3_0^9	37205	84	6	10	52	40	7	1	0	0
3_0^{10}	37774	80	8	12	35	45	16	4	1	0
3_0^{13}	39384	73	17	10	19	15	20	28	14	4
$3_0^5 5_0^1$	36268	84	2	14	87	11	1	0	0	0
$3_0^6 5_0^1$	36842	88	2	10	80	17	1	0	0	0

The most thermodynamically favored channel, $CH_2O + H$, is 68 kcal/mol lower in energy than channel (1). We cannot detect both of these fragments in coincidence because of the disparate mass ratio of 30:1, but the presence of this channel is observable in a simple fragment time-of-flight spectrum. In such an experiment on the 3_0^8 and 3_0^{10} bands of CD_3O [3], a small amount of deuterium atoms are observed, and we find that $2\%^{+5}_{-1}$ and $10\%^{+10}_{-5}$ of the radicals dissociate through channel (3) in these bands, respectively. In making this measurement, the geometric acceptance of the detector is calculated and corrected for as usual. Because of the deuterium atom's low laboratory energy of 470 eV, we estimate that it will be detected only 25% as efficiently as heavier fragments. The roughness of this estimate is reflected in the error bars on the branching ratios. Because this pathway is by far the most statistically favored channel for dissociation on the ground state, its small contribution to the overall fragmentation indicates that the other channels proceed on excited state surfaces.

For the $CH_3 + O$ channel, Table 1 shows that a high fraction of the available energy goes into translation for all transitions studied. The CH_3 photofragment vibrational distributions in Table 1 for the six 3_0^n transitions show that as the excitation energy is increased, the average energy in the CH_3 ν_2 mode increases. The CH_3 ($\nu_2 = 0$) state dominates the photofragment vibrational distributions, except for the 3_0^{10} and 3_0^{13} transitions, which yield inverted CH_3 population distributions. The non-inverted CH_3 ν_2 distributions for the 3_0^6–3_0^9 transitions resemble recent results obtained for CH_3I photodissociation [26]. The small amount of vibrational excitation in both systems indicates that dissociation is reasonably adiabatic on the repulsive surfaces, with the CH_3 group moving smoothly toward planar geometry as the bond breaks. However, this picture becomes less appropriate for CH_3O at higher excitation energies, where the inverted distribution is closer to what would be expected from a more impulsive dissociation process. Table 1 shows evidence for state-specificity in the CH_3 vibrational distributions. Even though the $3_0^6 5_0^1$ transition accesses a level with higher total energy than the 3_0^8 transition, the CH_3 distribution from the first transition is colder. It appears that energy in the ν_3 mode (the C–O stretch) of the $\tilde{A}$ state is the most important factor in determining the CH_3 vibrational distribution.

The remaining internal energy of the fragments must be partitioned between rotation of the methyl radical and the spin–orbit levels of the ^3P_j oxygen atom. Even in the case where no energy goes into oxygen spin–orbit excitation, the small fraction of the total energy in product rotation for the 3_0^7–3_0^{13} transitions implies that there is little torque along the potential surfaces involved in the dissociation.

While less information can be obtained for channel (2), it probably occurs through an excited state isomerization to CH_2OH. The $\tilde{X}(^3B_1)$ and $\tilde{a}(^1A_1)$ states of the CH_2 fragment, which are separated by 0.4 eV, are both energetically allowed as shown in Fig. 2. Although some ground state methylene may be produced, the data are consistent with a mecha-

[3] CD_3O was chosen because deuterium atoms have a higher detection efficiency than hydrogen atoms.

nism in which most or all of the CH_2 is in the excited singlet state.

In addition to the dynamical information obtained from this work, the bond dissociation energy, $D_0(CH_3–O)$, from our kinetic energy spectra yields many other thermodynamic quantities of interest. We find $\Delta H^0_{f,0}(CH_3O) = 6.8 \pm 0.4$ kcal/mol and $\Delta H^0_{f,298}(CH_3O) = 4.9 \pm 0.4$, where the change in enthalpy from 0 to 298 K follows Ruscic and Berkowitz [27]. This value agrees with an ab initio calculation of $\Delta H^0_{f,0}(CH_3O) = 6.6$ kcal/mol by Curtiss et al. [28], but is at least 1 kcal/mol higher than previous experimental values determined through kinetics, photoionization measurements [27,29–31] and from a recent compilation [32]. The straightforward method of extracting bond strengths from these data leads to the relatively small uncertainty in $\Delta H^0_{f,0}(CH_3O)$.

This improved value for the heat of formation allows us to obtain a value for the bond dissociation energy of the acidic hydrogen in methanol, $D_0(CH_3O–H) = 104.0 \pm 0.5$ kcal/mol, which agrees with a recent calculation of 105.0 ± 2 kcal/mol by Bauschlicher et al. [33] and an experimental determination of 104.0 ± 0.5 kcal/mol by Batt and McCulloch [30]. Using this bond strength, the ionization potential of H, and the electron affinity [21] of CH_3O^-, the gas phase acidity of methanol is found to be $\Delta H_{acid,0}(CH_3O–H) = 381.4 \pm 0.7$ kcal/mol, in agreement with recent work [32]. The C–H bond strength in CH_3O can be calculated in a similar manner: $D_0(H–CH_2O) = 19.8 \pm 0.4$ kcal/mol, which is consistent with previous determinations of 20 ± 3 [14] and 21 ± 1 [32] kcal/mol.

Finally, we obtain from this work a direct measure of the threshold for predissociation. We find that levels of the $\tilde{A}$ state are strongly predissociated starting with $\nu_3 = 6$ at 35419 cm^{-1} excitation energy, a value which is lower than several previous indirect determinations. Based on constant fluorescence lifetimes for decay of the $\tilde{A}$ state $\nu_3 = 0–6$ levels (31540–35354 cm^{-1}), Inoue et al. [6] proposed that the repulsive curve responsible for predissociation crosses the $\tilde{A}$ state above $\nu_3 = 6$. Fuke et al. [7] placed the curve crossing at 36800 ± 100 cm^{-1}, noting a sharp decrease in LIF signal above this energy. Further fluorescence lifetime measurements by Lin and Lee [13] led to an estimation of 36220 cm^{-1} as the predissociation threshold. In ab initio calculations, Jackels [16] predicted the lowest curve crossing to be 36500 cm^{-1}, slightly above $\nu_3 = 7$. Because we detect a signal *only* if the parent radical undergoes photofragmentation, the total photodissociation cross section spectrum shown in Fig. 1 demonstrates unambiguously that CH_3O $\tilde{A}(^2A_1)$ predissociates strongly above $E = 35400$ cm^{-1}.

In summary, we have measured the photofragment translational energy, angle, and mass distributions from predissociation in the methoxy radical $\tilde{A}(^2A_1) \leftarrow \tilde{X}(^2E)$ transition. Total dissociation cross section measurements show two strongly predissociated vibrational progressions, 3_0^n ($n = 6–13$) and $3_0^n 5_0^1$ ($n = 4–9$) with a dissociation threshold of $E = 35400$ cm^{-1}. The $P(E_T)$ distributions show resolved vibrational structure peaked near maximum E_T for the major product channel, C–O bond fission. These results imply relatively cold methyl radicals and a mechanism which, at least for the 3_0^n transitions ($n > 6$), maintains C_{3v} symmetry. A second product channel, $CH_2 + OH$, first appears at $E \approx 37800$ cm^{-1}, with a $P(E_T)$ which peaks at or near zero energy. The third product channel, loss of hydrogen, occurs from excitation of the 3_0^8 and 3_0^{10} transitions in CD_3O. A value for $D_0(CH_3–O)$ is found directly from the data, which provides new determinations of many thermodynamic quantities.

This research is supported by the Director, Office of Energy Research, Office of Basic Energy Sciences, Chemical Sciences Division of the US Department of Energy under Contract No. DE-AC03-76SF00098.

References

[1] D.W.G. Style and J.C. Ward, Trans. Faraday Soc. 49 (1953) 999.
[2] D.K. Russell and H.E. Radford, J. Chem. Phys. 72 (1980) 2750.
[3] Y. Endo, S. Saito, and E. Hirota, J. Chem. Phys. 81 (1984) 122.
[4] X. Liu, C.P. Damo, T.D. Lin, S.C. Foster, P. Misra, L. Yu and T.A. Miller, J. Phys. Chem. 93 (1989) 2266.
[5] H.R. Wendt and H.E. Hunziker, J. Chem. Phys. 71 (1979) 5202.
[6] G. Inoue, H. Akimoto and M. Okuda, J. Chem. Phys. 72 (1980) 1769.
[7] K. Fuke, K. Ozawa and K. Kaya, Chem. Phys. Letters 126 (1986) 119.

[8] S.D. Brossard, P.G. Carrick, E.L. Chappell, S.C. Hulegaard and P.C. Engelking, J. Chem. Phys. 84 (1986) 2459.
[9] S.C. Foster, P. Misra, T.D. Lin, C.P. Damo, C.C. Carter and T.A. Miller, J. Phys. Chem. 92 (1988) 5914.
[10] P. Misra, X. Zhu and C. Hsueh, Chem. Phys. 178 (1993) 377.
[11] Y.Y. Lee, G.H. Wann and Y.P. Lee, J. Chem. Phys. 99 (1993) 9465.
[12] D.E. Powers, J.B. Hopkins and R.E. Smalley, J. Phys. Chem. 85 (1981) 2711.
[13] S.R. Lin and Y.P. Lee, J. Chem. Phys. 88 (1988) 171.
[14] A. Geers, J. Kappert, F. Temps and J.W. Wiebrecht, J. Chem. Phys. 99 (1993) 2271.
[15] C.K. Westbrook and F.L. Dryer, Progr. Energy Combustion Sci. 10 (1984) 1.
[16] C.F. Jackels, J. Chem. Phys. 76 (1982) 505; 82 (1985) 311.
[17] A.G. Gaydon and H.G. Wolfhard, Proc. Roy. Soc. London A 208 (1951) 63.
[18] R.E. Continetti, D.R. Cyr, R.B. Metz and D.M. Neumark, Chem. Phys. Letters 182 (1991) 406.
[19] D.R. Cyr, R.E. Continetti, R.B. Metz, D.L. Osborn and D.M. Neumark, J. Chem. Phys. 97 (1992) 4937.
[20] R.E. Continetti, D.R. Cyr, D.L. Osborn, D.J. Leahy and D.M. Neumark, J. Chem. Phys. 99 (1993) 2616.
[21] P.C. Engelking, G.B. Ellison and W.C. Lineberger, J. Chem. Phys. 69 (1978) 1826.
[22] D.P. DeBruijn and J. Los, Rev. Sci. Instr. 53 (1982) 1020.
[23] R.N. Zare, Mol. Photochem. 4 (1972) 1.
[24] S. Yang and R. Bersohn, J. Chem. Phys. 61 (1974) 4400.
[25] T. Suzuki and E. Hirota, J. Chem. Phys. 98 (1993) 2387.
[26] G.E. Hall, T.J. Sears and J.M. Frye, J. Chem. Phys. 90 (1989) 6234;
T. Suzuki, H. Kanamori and E. Hirota, J. Chem. Phys. 94 (1991) 6607;
M. Zahedi, J.A. Harrison and J.W. Nibler, J. Chem. Phys. 100 (1994) 4043.
[27] B. Ruscic and J. Berkowitz, J. Chem. Phys. 95 (1991) 4033.
[28] L.A. Curtiss, L.D. Kock and J.A. Pople, J. Chem. Phys. 95 (1991) 4040.
[29] V.P. Glushko, L.V. Gurvich, G.A. Bergman, I.V. Veitz, V.A. Medredev, G.A. Khachkuruzov and V.C. Yungman, Termodinamicheskie cvoistva Individual'nikh veshchestv, Vols. 1, 2 (Nauka, Moscow, 1978/1979).
[30] L. Batt and R.D. McCulloch, Intern. J. Chem. Kinetics 8 (1976) 491.
[31] S.-C. Kuo, Z. Zhang, R.B. Klemm, J.F. Liebman, L.J. Stief and F.L. Nesbitt, J. Phys. Chem. 98 (1994) 4026.
[32] J. Berkowitz, G.B. Ellison and D. Gutman, J. Phys. Chem. 98 (1994) 2744.
[33] C.W. Bauschlicher Jr., S.R. Langhoff and S.P. Walch, J. Chem. Phys. 96 (1992) 450.